Published in final edited form as:
Comput Mech. 2014 March 1; 53(3): 403–412. doi:10.1007/s00466-013-0968-y.

Computational modeling of magnetic nanoparticle targeting to stent surface under high gradient field

Shunqiang Wang[1,‡], **Yihua Zhou**[1,‡], **Jifu Tan**[1], **Jiang Xu**[3], **Jie Yang**[3,*], and **Yaling Liu**[1,2,3,*]

[1]Department of Mechanical Engineering and Mechanics, Lehigh University, Bethlehem, PA, 18015

[2]Bioengineering Program, Lehigh University, Bethlehem, PA, 18015

[3]School of Mechanics and Engineering, Southwest Jiaotong University, Chengdu, China

Abstract

A multi-physics model was developed to study the delivery of magnetic nanoparticles (MNPs) to the stent-implanted region under an external magnetic field. The model is firstly validated by experimental work in literature. Then, effects of external magnetic field strength, magnetic particle size, and flow velocity on MNPs' targeting and binding have been analyzed through a parametric study. Two new dimensionless numbers were introduced to characterize relative effects of Brownian motion (BM), magnetic force induced particle motion, and convective blood flow on MNPs motion. It was found that larger magnetic field strength, bigger MNP size, and slower flow velocity increase the capture efficiency of MNPs. The distribution of captured MNPs on the vessel along axial and azimuthal directions was also discussed. Results showed that the MNPs density decreased exponentially along axial direction after one-dose injection while it was uniform along azimuthal direction in the whole stented region (averaged over all sections). For the beginning section of the stented region, the density ratio distribution of captured MNPs along azimuthal direction is center-symmetrical, corresponding to the center-symmetrical distribution of magnetic force in that section. Two different generation mechanisms are revealed to form four main attraction regions. These results could serve as guidelines to design a better magnetic drug delivery system.

Keywords

targeted delivery; magnetic nano-particles; magnetic force; particle size; magnetic stent

Introduction

Magnetic nanoparticles (MNPs) have been widely used in many bio-medicine applications such as drug delivery, drug releasing, and cancer diagnosis [1–5]. It is a promising technique for curing diseases like cancer [2], local injury [6,7], or local cell proliferation [8]. By applying an external magnetic field, the drug-carried MNPs can be targeted to the region of interest to avoid full circulation in human body, reduce the curing time, and minimize dosages and side effects. The technique of MNP targeting mainly consists of two parts: loading drugs to MNPs and capturing them via an external magnetic field to a targeted region. The latter is the focus of this paper.

*Corresponding authors. Tel.: +1-610-758-5839; fax: +1-610-758-6224. yal310@lehigh.edu (Y. Liu).
yangchenjie@home.swjtu.edu.cn (J. Yang).
‡These authors contribute equally to this work

Experimental work on MNPs targeting has been carried out in research and clinic applications. Various MNPs have been synthesized [9]. MNPs' fabrication process, physical principles of magnetic targeting, and obstacles to the clinical applications have been summarized by Yigit *et al.* [2]. A few simulation works have also been carried out. Finite element methods (FEMs) have been widely used to investigate the motion of NPs under different physical conditions [10–14]. Wong *et al.* [15] applied FEM simulations of magnetic particle inspection to analyze the magnetic field around a defect. Furlani *et al.* [16] developed a FEM model to predict the capture of magnetic micro/nano-particles in a bioseparation microsystem. Furlani [17] pointed out that FEM was typically used to determine the magnetic field and force when studying particles transport.

Based on studies of previous researchers, the targeting method of MNPs still needs to be improved due to its limited capture efficiency. Forbes *et al.* [18] proposed a novel approach that used a magnetizable stent to achieve efficient targeted drug delivery. Two independent sources of the magnetic field are exerted on MNPs to make them better captured on regions of interest and also allow deep penetration within the subject: one is external high gradient magnetic field to attract the magnetic drug carriers to the stent, the other one is the magnetic field induced by the magnetized stent. This approach can not only improve the capture efficiency of MNPs in the injury region of interest but also solve one of major problems caused by stent-restenosis [19], because MNPs can constantly and quantitatively provide anti-proliferative agents. It offers a new approach for restenosis treatment and MNPs accumulation. Later, Polyak *et al.* [20], Chorny *et al.* [8,21–23] and other researchers [24] carried out a series of studies to verify and improve this method. However, their work only proved the feasibility of this approach. Quantitative analysis of magnetic drug delivery system design combined with stents is still needed to obtain better capture efficiency of MNPs. The goal of our work is to characterize the effects of external magnetic field, MNP size, and flow velocity on the capturing of MNPs. Meanwhile, unveiling the mechanism of how the magnetic force influences the capturing of MNPs can provide a better understanding of targeted MNP delivery.

In this paper, a finite element model of MNP binding on stent is firstly developed and verified by experimental results in Forbe's work [18]. Then, effects of external magnetic field, MNP size and flow velocity on capturing of MNPs are discussed by using the presented model. Two dimensionless numbers are introduced to characterize effects of these three factors on MNPs transport. Lastly, a general case is built to study the specific distribution of captured MNPs along the stented region. The mechanism of magnetic force in localized regions is unveiled and it reveals that magnetic force can either attract MNPs towards or repel MNPs away from the stented surface.

Methods

(1) Model description

The channel with a diameter of 3 mm [25] and a length of 20 mm is built to represent the blood vessel. The Palmaz-Schatz type of stent [26–29] with a length of 15 mm is implanted in the middle of channel, embedded into the channel wall tightly. The inner diameter of the stent is 3 mm, same as the channel diameter; the outer diameter of stent is 3.2 mm. Incompressible fluid flow and magnetic field are applied to the system. The whole problem is solved using FEM approach. The mesh elements used in the work are tetrahedral with a minimum element quality of 0.3278 for the whole domain. Finer meshes are applied in the stent and other regions close to the stent. Moreover, four times of mesh elements have been applied and differences within 2% are observed for both pressure and magnetic field. Thus, this mesh setup can guarantee the correctness of our simulation results.

(2) Flow field

The blood flow is considered to have a density of 1060 kg/m^3 [30] and a dynamic viscosity of 4×10^{-3} Pa·s [31]. The flow is assumed to be fully developed in the blood. For the pressure at outlet, from Navier-stokes equations, only the pressure gradient influences the velocity of fluid flow. Thus, as long as the pressure gradient is fixed, the outlet pressure can be chosen as a reference pressure, which is expressed as 0 Pa in the model. Based on $\frac{dp}{dy}=-\frac{32\mu u_{ave}}{d^2}$ for a pipe flow, the analytical pressure gradient is specified as −355.6 Pa/m, −711.1 Pa/m, −2133.3 Pa/m, −3555.6 Pa/m and −4977.8 Pa/m, which correspond to peak flow velocity of 0.05 m/s, 0.1 m/s, 0.3 m/s, 0.5 m/s and 0.7 m/s (introduced in section (7)), respectively. However, in our numerical model, the pressure gradient is not imposed and it is a result of simulation which relies on the simulation accuracy. In order to verify that our numerical model has a reliable simulation accuracy, the typical case of peak flow velocity of 0.1 m/s is considered. The exact analytical pressure gradient is −711.1 Pa/m, while the computed pressure gradient is −705.0 Pa/m. With the difference of 0.86%, it is demonstrated that the simulation results can well mimic the actual fluid field based on analytical solution.

The stent is tightly embedded into the artery wall so it doesn't affect the flow velocity. The flow in the channel is treated as Newtonian, incompressible, fully developed and steady. The flow field is simulated by solving the Navier-Stokes equation:

$$\rho\left(\frac{\partial \boldsymbol{u}}{\partial t}+\boldsymbol{u}\cdot\nabla\boldsymbol{u}\right)=-\nabla p+\mu\nabla^2\boldsymbol{u} \quad (1)$$

$$\nabla\cdot\boldsymbol{u}=\mathbf{o} \quad (2)$$

where $\boldsymbol{u}$ is the fluid velocity in the fluid domain, ρ and μ are density and viscosity of the fluid respectively, p is the hydraulic pressure in the fluid domain, and t stands for time.

(3) Magnetic field

A uniform external magnetic field is applied to the model in Z direction. A 6 mm×20 mm×6 mm box is created to represent the external environment of the vessel including human tissues and air. It is challenging to take all components of human tissues, such as bone, fat, muscle, etc., into account in magnetic field modeling. Thus, following others' approaches [32–34], the intra-tissue permeability differences are not considered and all tissues are treated as water. The relative permeability of water is 0.999992, which is close to 1.0000004 for air. The material of stent is 304 grade stainless steel with a relative permeability of 1.8 [22]. Uniform magnetic flux density in Z direction is applied to the system. The four faces of the box in X and Y direction are set as magnetic insulation for an ideal uniform magnetic field. The magnetic field distribution is simulated by solving the magnetostatics equation, a special case of Maxwell's equations:

$$-\nabla\cdot\mu_0\mu_{\mathrm{r}}\nabla V_m=0 \quad (3)$$

Where μ_0 is the permeability constant with a value of $-4\pi\times10^{-7}$ H·m^{-1}, μ_r is the relative permeability of medium, and V_m is the magnetic potential.

(4) Mathematical model for MNPs

A multi-physics model is developed to study the transport of MNPs to the targeted stented region in the magnetic field. The motion of MNP is dominated by the magnetic force, fluid drag force and thermal kinetic force induced by Brownian motion (BM). These forces are

typically in the order of 10^{-1} or a few pN. However, inertia force, gravitational force and buoyancy force are neglected due to their small magnitude (typically in the order of 10^{-4} pN) compared to dominant forces listed above [35–39]. Other factors such as cell-particle and particle-particle interaction forces will make our model complex and they are also computationally too expensive to be included in our large scale stent model [40]. These factors are studied in our previous work [40,41] about nanoparticle delivery in microcirculation, but are not considered in this paper. A uniform external magnetic field is applied in 3D model, while both MNPs and the implanted stent are paramagnetic. One dose of MNPs is injected into the artery and trajectories of MNPs are described by the following governing equation:

$$m_{MNP}\dot{\boldsymbol{u}}_{MNP}=\boldsymbol{F}_{MNP}+\boldsymbol{F}_f+\boldsymbol{F}_B=0 \quad (4)$$

where $\boldsymbol{F}_{MNP}$ is the magnetic force applied on the MNP, $\boldsymbol{F}_f$ the fluid drag force and $\boldsymbol{F}_B$ the force due to BM. m_{MNP} and $\dot{\boldsymbol{u}}_{MNP}$ are the mass and velocity of MNPs, respectively. Details about how to consider these three forces in eq. (4) are introduced as follows.

The fluid drag force is calculated using Stokes' approximation for a spherical particle in laminar flow [42]:

$$\boldsymbol{F}_f=C_d(\boldsymbol{u}-\boldsymbol{u}_{MNP}) \quad (5)$$

where $C_d = 6\pi\mu r_{MNP}$ is the drag coefficient, where r_{MNP} is the radius of the MNPs.

Displacement induced by BM is directly calculated using traditional diffusion theory expressed as:

$$\langle|\boldsymbol{r}|^2\rangle=6Dt \quad (6)$$

where $\langle\ \rangle$ means the time average, $\boldsymbol{r}$ is the position vector of MNPs, D for the diffusion coefficient which is formulated as $D=\frac{kT}{6\pi\mu r_{MNP}}$, where k and T are Boltzmann constant and temperature, respectively.

A mathematic model is developed to describe the magnetic characteristics of MNPs and the magnetic field which is the superposition of applied external uniform magnetic field and non-uniform field induced by the magnetized stent. Here MNP is treated as an equivalent magnetic point dipole through an effective dipole moment approach [43]. For a paramagnetic sphere, the magnetic moment $\boldsymbol{m}$ of the point dipole is aligned with the external magnetic field:

$$\boldsymbol{m}=\frac{\chi_{MNP}}{1+D_{MNP}\chi_{MNP}}V\boldsymbol{H} \quad (7)$$

where $\boldsymbol{H}$ is the total magnetic field strength applied on the center of MNP, V is the volume of the MNP, D_{MNP} is the demagnetization coefficient (D_{MNP} = 1/3 for a sphere), χ_{MNP} and μ_{MNP} are the susceptibility and permeability of MNPs respectively with a relationship of $\chi_{MNP} = \mu_{MNP}^{-1}$.

The magnetic force is calculated as: $\boldsymbol{F}_{MNP} = (\boldsymbol{m}\bullet\nabla)\,\boldsymbol{B} = \mu_0\,(\boldsymbol{m}\bullet\nabla)\,\boldsymbol{H}$ [44]. The formula of the magnetic force is expanded to calculate the component of magnetic force in i direction, where i could be x, y or z:

$$F_{MNPi}=\mu_0\left(m_x\frac{\partial H_i}{\partial x}+m_y\frac{\partial H_i}{\partial y}+m_z\frac{\partial H_i}{\partial z}\right) \quad (8)$$

Where m_x, m_y and m_z are the components of magnetic moments in *x*, *y* and z direction respectively. H_i is the component of magnetic field in *i* direction. Accordingly, the velocity component in *i* direction induced by magnetic force is calculated based on Stokes' law as:

$$u_{MNPi}=\frac{F_{MNPi}}{6\pi\mu r_{MNP}} \quad (9)$$

(5) Model validation with experimental results

To further verify this model, simulated results are compared with experimental data reported in Ref. [18]. In Forbe's experimental work [18], capture efficiency on stents, which is defined as the ratio between the amount of captured MNPs in the stented region and overall MNPs released, with different relative permeability is presented. In our numerical model, MNPs with a distance to the stent smaller than their radius are treated to be captured. Validation of our current numerical model is performed by comparing our numerical results with the experimental results. Details of the numerical model are provided as follows. The whole setup of the system is the same as the one shown in Fig. 1. A few minor changes are made to make numerical simulation consistent with experimental work. Specifically, the stent used in [18] is 5 mm in diameter and 20 mm in length. The blood vessel embedded with stent is also extended correspondingly. The diameter of the wire is 150 μm. The external uniform magnetic field is set as 0.05 T. The peak flow velocity at inlet is set as 0.2 m/s, which is a typical value for artery [10]. Diameter and susceptibility for MNPs are set as 350 nm and 1 (in the order of ~1–2), respectively. Material of the stent is 304 grade stainless steel with relative permeability of 1.80, 6.94 and 10.44, which correspond to different thicknesses of plated magnetic material.

Based on our numerical model setup proposed above, transport of MNPs is determined and results on capture efficiency in different cases are obtained. Comparison between numerical and experimental results is shown in Fig. 2. Results show that the capture efficiency on stents of various relative permeability is consistent between numerical and experimental cases, although difference in absolute values exists. These differences could be due to several reasons. Firstly, the experimental work considered an *in vivo* test, where MNPs can also be captured on non-targeted regions, thus decreasing the amount of MNPs entering the stented blood vessel. The resulting capture efficiency in experiments becomes smaller. Secondly, other factors such as blood cells, non-uniform vessel geometry, and pulsatile blood flow may also contribute to this difference. With that, the rate of change for capture efficiency in terms of relative permeability is also calculated for both numerical and experimental models to demonstrate the validation of our model. Cases of μ_r equal to 6.94 and 10.44 are considered with the case of μ_r=1.8 as the reference. As shown in the inset of Fig. 2, the rate of change for capture efficiency agrees very well between the modeling results and experimental results. Thus, the model provides insights on how relative permeability of stent influences the capture efficiency qualitatively.

(6) Initial settings of MNPs

According to Ref. [8], if the distance between the wall and MNP is bigger than 50 um, the influence of the local high gradient magnetic field induced by the stent on MNPs can be ignored. Thus, all MNPs are released in the vicinity of stent surface with an initial distance

of smaller than 50 um. In each case, 824 MNPs, with a same surface concentration of $1.8 \times 10^{10}/m^2$ reported in Ref. [45], are released at the inlet and transported within the blood flow under effects of magnetic force, drag force and Brownian motion. The magnetic susceptibility of MNPs is 0.27 [8].

(7) Selection of parameters

The magnetic field strength is selected as 0 T, 0.01 T, 0.5 T, 2 T, 6 T and 8 T within the FDA suggested range [46]. Based on the organ filtration mechanism, particles bigger than 200 nm are readily filtered by liver and spleen while those smaller than 10 nm are easily cleared by the kidney or through extravasations during the blood circulation [47,48]. So the radius of MNPs is chosen as 25 nm, 50 nm, 100 nm and 150 nm. A case of 500 nm is also added for the comparison purpose. Peak velocity of the inlet parabolic flow is chosen as 0.05 m/s, 0.1 m/s, 0.3 m/s, 0.5 m/s and 0.7 m/s [10], with corresponding shear rate of 67 /s, 133 /s, 400 /s, 667 /s and 933 /s, respectively (based on the formula $\dot{\gamma}=\frac{8u_{ave}}{d}$, where u_{ave} is the average blood flow and d is the diameter of the blood vessel).

Two dimensionless numbers β_m and Pe_m are created to evaluate relative effects of BM, magnetic force induced particle motion and convective blood flow. β_m measures the ratio of the time for particles to reach the wall by diffusion to that by magnetic force.

$$\beta_m=\frac{{d_c}^2/6D}{d_c/u_m}=\frac{d_c u_m}{6D} \quad (10)$$

where d_c is the capture distance, which is chosen to be 50 um as mentioned above, D is the diffusion coefficient, and u_m is the magnetic field induced velocity in the normal direction of the stent surface. $\beta_m>>1$ indicates that the capture process of MNPs is magnetic force dominated. $\beta_m<<1$ indicates that the capture process of MNPs is diffusion dominated.

Meanwhile, Pe_m is a modified Peclet number characterizing the ratio between MNP radial traveling time toward the wall and the convection time in the channel. It evaluates whether the flushing effect or capturing effect is dominant in the particle delivery.

$$Pe_m=\frac{d_c/(6D/d_c+u_m)}{L/U}=\frac{{d_c}^2 U}{L(6D+u_m d_c)} \quad (11)$$

where U is the characteristic convection velocity in the region away from the wall with a distance of d_c, and L is the characteristic length and chosen as the length of stent in this case.

Pe_m can also be expressed by another dimensionless number Reynolds number Re as:

$$Pe_m=\frac{{d_c}^2 \mu \mathrm{Re}}{\rho d L(6D+u_m d_c)} \quad (12)$$

where $\mathrm{Re}=\frac{\rho u_{ave} d}{\mu}$ and d is the diameter of the vessel. Among the three factors (magnetic field strength, diameter of the MNPs and fluid velocity) studied in this work, Re is only influenced by flow velocity. Since fluid velocity effect is already considered in Pe_m, a separate discussion on Re is not provided.

After the release, particles are transported in the channel under effects of external magnetic field, high gradient magnetic field induced by the stent, flow drag force, and BM. When distances between MNPs and the artery wall are smaller than MNPs' radius, they are treated to be captured by the stented region.

Results and Discussion

In consideration of the case of the flow rate as 0.7 m/s and the magnetic flux density as 2 T, the simulation results of velocity in the channel and the system's magnetic flux density are shown in Fig. 3.

The capture efficiency of MNPs α is defined as the fraction of captured MNPs over those injected from the inlet. In the following session, the effects of magnetic field, MNP size and flow velocity on capture efficiency are studied. β_m and Pe_m are analyzed to evaluate the relative dominant effect of MNPs motion in each case. The distribution of captured MNPs is studied along axial and azimuthal directions.

Fig. 4(a) shows the capture efficiency under various magnetic fields. The flow velocity is set as 0.1 m/s and the radius of particles is 100 nm. The magnetic field strength is set as 0 T at first to prove the feasibility and high efficiency of capture of MNPs under magnetic field. The capture efficiency without magnetic field is 6% while it reaches 79% under the magnetic field strength of 6 T. Furthermore, in the range of weak magnetic fields, namely from 0.01 T to 2 T, the capture efficiency increases rapidly with magnetic field, reaching 58% under magnetic field strength of 2 T. Capture efficiency reaches a saturation value of 80% when magnetic field reaches 8 T. The saturation is also observed by other researchers [45]. The enhancement of capture efficiency induced by magnetic fields can be explained through Fig. 4(b). β_m increases with larger magnetic field strength, indicating a more significant impact of magnetic force on MNPs motion with larger magnetic field strength. More MNPs are attracted to the wall and the capture efficiency increases correspondingly under a higher magnetic field strength. As for Pe_m, it decreases with increasing magnetic fields, leading to a faster capturing process because the enhanced magnetic force pulls MNPs towards the stented region faster.

The effects of particle size on the capture efficiency are shown in Fig. 5(a). The capture efficiency increases with increased particle size. In this case β_m is always larger than 1 as shown in Fig. 5(b), which means this process is always magnetic force dominated. From Eq. (7)–(10), magnetic force and β_m are proportional to r^3 which verifies that β_m increases with the particle size. Referring to Eq. (9), u_m is proportional to r^2. As a result, with r increasing, the transport time to the wall decreases as the velocity component induced by magnetic force increases. Meanwhile, the increase of u_m with particle size leads to a decrease of Pe_m. The decreasing trend of Pe_m indicates that MNPs tend to be pulled to the stent surface, resulting in an increased capture efficiency.

Fig. 6(a) shows the trend of capture efficiency under various flow velocities. It demonstrates that the capture efficiency decreases as the flow velocity increases, since higher flow velocity gives MNPs less time to enter the captured region and a higher chance to be flushed away. Fig. 6(b) indicates that β_m is not a function of flow velocity based on Eq. (10). As for Pe_m, it increases because the convection time of MNPs decreases due to the increased flow velocity. In other words, more MNPs are flushed away, resulting in a decreased capture efficiency.

To study the distribution of captured MNPs in axial and azimuthal direction, a general case is studied with the parameters of $B = 1\ T$, $r = 100\ nm$, $u = 0.1\ m/s$. The distribution of

captured MNPs in the whole stented region is shown in Fig. 7, while the distribution of MNPs and the magnetic force distribution in the beginning section of the stent section are displayed in Fig. 8.

As shown in Fig. 7(a), the number of captured MNPs along the axial direction decreases exponentially because only one dose of MNPs are injected into the model, resulting in decreased free particle concentration along the vessel. However, the distribution of MNPs along the azimuthal direction in the whole stented region is uniform (averaged over all sections), which can be explained by the uniform distribution of the stent structure and average magnetic force along the azimuthal direction.

As shown in Fig. 8(b), the distribution of captured MNPs in azimuthal direction is center-symmetrical in the beginning section of the stented region, while they are uniformly distributed for the whole stented region, as shown in Fig. 7(d). This center-symmetrical distribution of captured MNPs is corresponding to the center-symmetrical distribution of magnetic force, as shown in Fig. 8(a). In this case, $\beta_m = 2.12\times10^3$ implies that this is a magnetic force dominated case. Magnetic force can act as either attraction or repulsion for MNPs, which depends on whether its radial direction component points to the stent surface or points to the channel center. If the radial direction component of magnetic force points to the stent surface, the magnetic force acts as an attraction; if it points to the channel center, the magnetic force acts as the repulsion respectively. From Fig. 8(b), 60% of captured MNPs are concentrated in four main attraction regions named as ①–④, and much less MNPs are captured in other regions. The generation mechanisms of these attraction regions are different. For region ① & ③ which are located between two stent struts, the local magnetic force is small, but the magnetic forces in the nearby vicinity are large and they act as repulsive forces. When particles are in the vicinity of these two regions, they are pushed into and captured in these two regions. In another word, the attraction region ① & ③ are formed indirectly by the repulsion of MNPs from nearby stent struts. On the other hand, the attraction region ② & ④ which are located on stent struts, are directly formed by the attraction of stent struts there. For region ② & ④, the accumulative local magnetic force acts as attractions even though both attractive and repulsive forces exist in each region. Thus, particles are attracted to these two attraction regions directly by magnetic force in these two regions.

Conclusion

A multi-physics computational model is developed and validated by experimental work in literature [18]. Then, effects of magnetic field, particle size and flow velocity on the capture efficiency of MNPs in the stented region are studied. The implanted paramagnetic stent generates large local magnetic force on the MNPs under the external magnetic field. The feasibility of this approach is validated by comparing capture efficiency of MNPs without magnetic field and that with magnetic field strength of 6 T. A parametric study was performed on the capture efficiency of MNPs. It is concluded that that larger magnetic field strength, bigger MNPs, and slower flow velocity enhance the MNPs capture efficiency. The magnetic force might either attract MNPs toward or repel MNPs away from the stent surface, depending on whether its force component in radial direction points to the stent surface or to the channel center. In addition, MNPs density decreases exponentially along the axial direction after one-dose injection while the distribution of captured MNPs along azimuthal direction is uniform in the whole stented region. A center-symmetrical distribution of captured MNPs is observed at beginning cross-section of the stent, with MNPs concentrated in four main attraction regions. Two generation mechanisms of attraction regions are revealed and explained by the distribution profile of magnetic force.

Such non-uniform MNPs distribution might be improved through the design of stent and the way magnetic field is applied, i.e., the application of a rotation magnetic field.

In the current model, an ideal velocity field in a circular blood vessel is used, while the influence of the deformed vessel caused by the expansion of stent is neglected. In the future, blood flow velocity in a more realistic stented vessel will be considered to provide more accurate predictions for nanoparticle delivery in stented region under clinical setup.

Acknowledgments

The authors acknowledge the supports of this work from National Institute of Health (Grant EB015105) and National Science Foundation (Grant CBET-1113040, CBET-1067502).

Reference

1. Chen GJ, Wang LF. Design of magnetic nanoparticles-assisted drug delivery system. Current pharmaceutical design. 2011; 17(22):2331–2351. [PubMed: 21736546]
2. Yigit MV, Moore A, Medarova Z. Magnetic Nanoparticles for Cancer Diagnosis and Therapy. Pharm Res-Dordr. 2012; 29(5):1180–1188.
3. Azhar SL, Lotfipour F. Magnetic nanoparticles for antimicrobial drug delivery. Die Pharmazie. 2012; 67(10):817–821. [PubMed: 23136713]
4. Park H, Yang J, Seo S, Kim K, Suh J, Kim D, Haam S, Yoo KH. Multifunctional nanoparticles for photothermally controlled drug delivery and magnetic resonance imaging enhancement. Small. 2008; 4(2):192–196. [PubMed: 18203232]
5. Dave SR, Gao X. Monodisperse magnetic nanoparticles for biodetection, imaging, and drug delivery: a versatile and evolving technology. Wiley interdisciplinary reviews Nanomedicine and nanobiotechnology. 2009; 1(6):583–609. [PubMed: 20049819]
6. McGill SL, Cuylear CL, Adolphi NL, Osinski M, Smyth HD. Magnetically responsive nanoparticles for drug delivery applications using low magnetic field strengths. IEEE transactions on nanobioscience. 2009; 8(1):33–42. [PubMed: 19304499]
7. Liu Y, Shah S, Tan J. Computational Modeling of Nanoparticle Targeted Drug Delivery. Reviews in Nanoscience and Nanotechnology. 2012; 1(1):66–83.
8. Chorny M, Fishbein I, Yellen BB, Alferiev IS, Bakay M, Ganta S, Adamo R, Amiji M, Friedman G, Levy RJ. Targeting stents with local delivery of paclitaxel-loaded magnetic nanoparticles using uniform fields. P Natl Acad Sci USA. 2010; 107(18):8346–8351.
9. Dobson J. Magnetic nanoparticles for drug delivery. Drug Develop Res. 2006; 67(1):55–60.
10. Grief AD, Richardson G. Mathematical modelling of magnetically targeted drug delivery. J Magn Magn Mater. 2005; 293(1):455–463.
11. Tzirtzilakis EE, Loukopoulos VC. Biofluid flow in a channel under the action of a uniform localized magnetic field. Comput Mech. 2005; 36(5):360–374.
12. Liu Y, Tan J, Thomas A, Ou-Yang D, Muzykantov VR. The shape of things to come: importance of design in nanotechnology for drug delivery. Therapeutic delivery. 2012; 3(2):181–194. [PubMed: 22834196]
13. Tan JF, Shah S, Thomas A, Ou-Yang HD, Liu YL. The influence of size, shape and vessel geometry on nanoparticle distribution. Microfluid Nanofluid. 2013; 14(1–2):77–87. [PubMed: 23554583]
14. Shah S, Liu YL, Hu W, Gao JM. Modeling Particle Shape-Dependent Dynamics in Nanomedicine. J Nanosci Nanotechno. 2011; 11(2):919–928.
15. Wong, BS.; Low, YG.; Xin, W.; Jee-Hou, H.; ChingSeong, T.; Jong Boon, O. 3D finite element simulation of magnetic particle inspection. Sustainable Utilization and Development in Engineering and Technology (STUDENT), 2010 IEEE Conference on; 20-21 Nov. 2010; 2010. p. 50-55.

16. Furlani EP, Sahoo Y, Ng KC, Wortman JC, Monk TE. A model for predicting magnetic particle capture in a microfluidic bioseparator. Biomed Microdevices. 2007; 9(4):451–463. [PubMed: 17516176]

17. Furlani EP. Analysis of particle transport in a magnetophoretic microsystem. J Appl Phys. 2006; 99(2) Artn 024912.

18. Forbes ZG, Yellen BB, Halverson DS, Fridman G, Barbee KA, Friedman G. Validation of high gradient magnetic field based drug delivery to magnetizable implants under flow. Ieee T Bio-Med Eng. 2008; 55(2):643–649.

19. Gay M, Zhang LT. Numerical studies of blood flow in healthy, stenosed, and stented carotid arteries. Int J Numer Meth Fl. 2009; 61(4):453–472.

20. Sensenig R, Sapir Y, MacDonald C, Cohen S, Polyak B. Magnetic nanoparticle-based approaches to locally target therapy and enhance tissue regeneration in vivo. Nanomedicine-Uk. 2012; 7(9): 1425–1442.

21. Chorny M, Fishbein I, Alferiev I, Levy RJ. Magnetically Responsive Biodegradable Nanoparticles Enhance Adenoviral Gene Transfer in Cultured Smooth Muscle and Endothelial Cells. Mol Pharmaceut. 2009; 6(5):1380–1387.

22. Polyak B, Fishbein I, Chorny M, Alferiev I, Williams D, Yellen B, Friedman G, Levy RJ. High field gradient targeting of magnetic nanoparticle-loaded endothelial cells to the surfaces of steel stents. Proc Natl Acad Sci U S A. 2008; 105(2):698–703. [PubMed: 18182491]

23. Chorny M, Polyak B, Alferiev IS, Walsh K, Friedman G, Levy RJ. Magnetically driven plasmid DNA delivery with biodegradable polymeric nanoparticles. FASEB journal : official publication of the Federation of American Societies for Experimental Biology. 2007; 21(10):2510–2519. [PubMed: 17403937]

24. Chorny M, Fishbein I, Forbes S, Alferiev I. Magnetic Nanoparticles for Targeted Vascular Delivery. Iubmb Life. 2011; 63(8):613–620. [PubMed: 21721100]

25. Forbes' DSH, ZG.; Fridman1, G.; Yellen2, BB.; Chomy3, M.; Friedman2, G.; Barbeel, KA. Locally targeted drug delivery to magnetic stents for therapeutic applications. IEEE/EMBS International Summer School on Medical Devices and Biosensors (ISSS-MD); 2004.

26. Liu, Y.; Yang, J.; Zhou, Y.; Hu, J. Multiscale Simulations and Mechanics of Biological Materials. John Wiley & Sons Ltd; 2013. Structure Design of Vascular Stents; p. 301-317.

27. Gay M, Zhang L, Liu WK. Stent modeling using immersed finite element method. Comput Method Appl M. 2006; 195(33–36):4358–4370.

28. Liu WK, Liu YL, Farrell D, Zhang L, Wang XS, Fukui Y, Patankar N, Zhang YJ, Bajaj C, Lee J, Hong JH, Chen XY, Hsu HY. Immersed finite element method and its applications to biological systems. Comput Method Appl M. 2006; 195(13–16):1722–1749.

29. Gay M, Zhang LT. Numerical studies on fluid-structure interactions of stent deployment and stented arteries. Eng Comput-Germany. 2009; 25(1):61–72.

30. Cutnell JJ, Kenneth. Density of blood. Physics. 1998

31. Erica, M.; Cherrya, JKE. Simulation of Magnetic Particles in the Bloodstream for Magnetic Drug Targeting Applications. 8th International Conference on Multiphase Flow; 2013.

32. Li SZ, Williams GD, Frisk TA, Arnold BW, Smith MB. A Computer-Simulation of the Static Magnetic-Field Distribution in the Human Head. Magnet Reson Med. 1995; 34(2):268–275.

33. Bhagwandien, R. Object Induced Geometry and Intensity Distortions in Magnetic Resonance Imaging: Met Een Samenvatting in Het Nederlands. Univerisiteit Utrecht, Faculteit Geneeskunde; 1994.

34. Li SZ, Dardzinski BJ, Collins CM, Yang QX, Smith MB. Three-dimensional mapping of the static magnetic field inside the human head. Magnet Reson Med. 1996; 36(5):705–714.

35. Dames P, Gleich B, Flemmer A, Hajek K, Seidl N, Wiekhorst F, Eberbeck D, Bittmann I, Bergemann C, Weyh T, Trahms L, Rosenecker J, Rudolph C. Targeted delivery of magnetic aerosol droplets to the lung. Nat Nanotechnol. 2007; 2(8):495–499. [PubMed: 18654347]

36. Alexandra, Heidsieck BG. Analysis of Particle Trajectories for Magnetic Drug Targeting. COMSOL conference; Paris. 2010. 2010

37. Gleich B, Hellwig N, Bridell H, Jurgons R, Seliger C, Alexiou C, Wolf B, Weyh T. Design and evaluation of magnetic fields for nanoparticle drug targeting in cancer. Ieee T Nanotechnol. 2007; 6(2):164–170.
38. Tan J, Wang S, Yang J, Liu Y. Coupled particulate and continuum model for nanoparticle targeted delivery. Computers & Structures. 2013; 122(0):128–134. http://dx.doi.org/10.1016/j.compstruc.2012.12.019. [PubMed: 23729869]
39. Liu YL, Guo QJ, Wang SQ, Hu W. Electrokinetic effects on detection time of nanowire biosensor. Appl Phys Lett. 2012; 100(15) Artn 153502.
40. Tan JF, Thomas A, Liu YL. Influence of red blood cells on nanoparticle targeted delivery in microcirculation. Soft Matter. 2012; 8(6):1934–1946. [PubMed: 22375153]
41. Liu YL, Oh K, Bai JG, Chang CL, Yeo W, Chung JH, Lee KH, Liu WK. Manipulation of nanoparticles and biomolecules by electric field and surface tension. Comput Method Appl M. 2008; 197(25–28):2156–2172.
42. Wasilewski J, Mirota K, Peryt-Stawiarska S, Nowakowski A, Polonski L, Zembala M. An introduction to computational fluid dynamics based on numerical simulation of pulsatile flow in the left coronary artery. Kardiochir Torakochi. 2012; 9(3):366–374.
43. Furlani EP, Ng KC. Analytical model of magnetic nanoparticle transport and capture in the microvasculature. Phys Rev E. 2006; 73(6) Artn 061919.
44. Shire, ES. Classical electricity and magnetism. Cambridge Eng: University Press; 1960.
45. Ravnik J, Hribersek M. High gradient magnetic particle separation in viscous flows by 3D BEM. Comput Mech. 2013; 51(4):465–474.
46. Zaremba LA. Guidance for Industry and FDA Staff: Criteria for Significant Risk Investigations of Magnetic Resonance Diagnostic Devices. Center for Devices and Radiological Health. 2003
47. Petros RA, DeSimone JM. Strategies in the design of nanoparticles for therapeutic applications. Nat Rev Drug Discov. 2010; 9(8):615–627. [PubMed: 20616808]
48. Wang J, Byrne JD, Napier ME, DeSimone JM. More Effective Nanomedicines through Particle Design. Small. 2011; 7(14):1919–1931. [PubMed: 21695781]

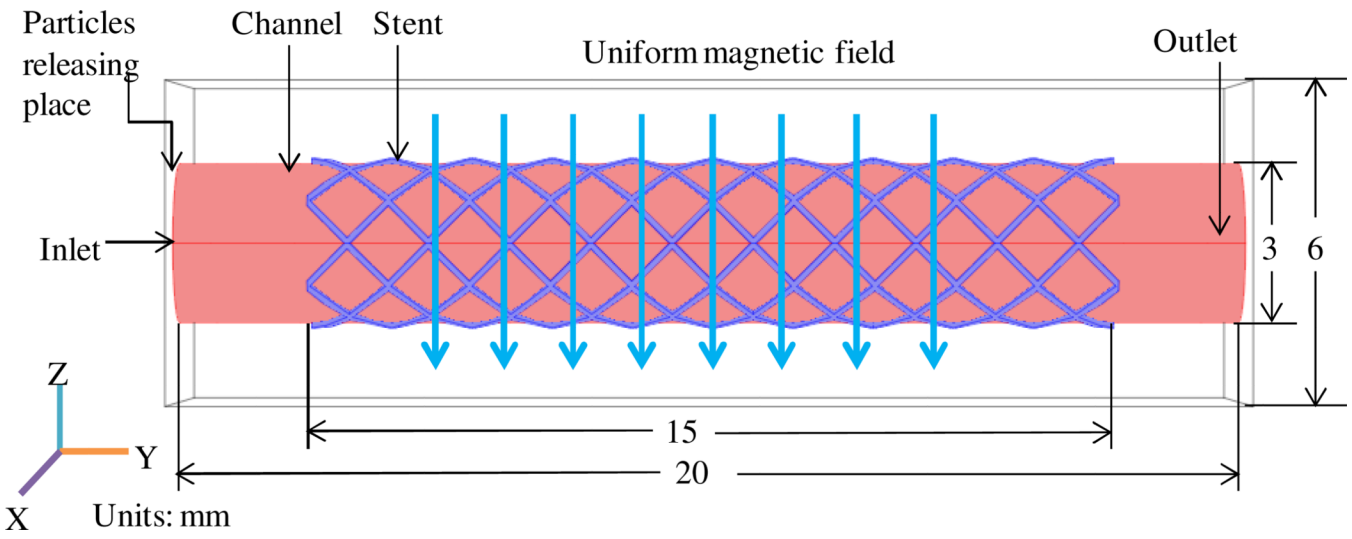

Fig. 1.
Setup of the system: a Palmaz-Schatz type of stent is embedded in a blood vessel. A uniform magnetic field along Z direction is applied in the system. MNPs are released from the inlet. The size unit is millimeter.

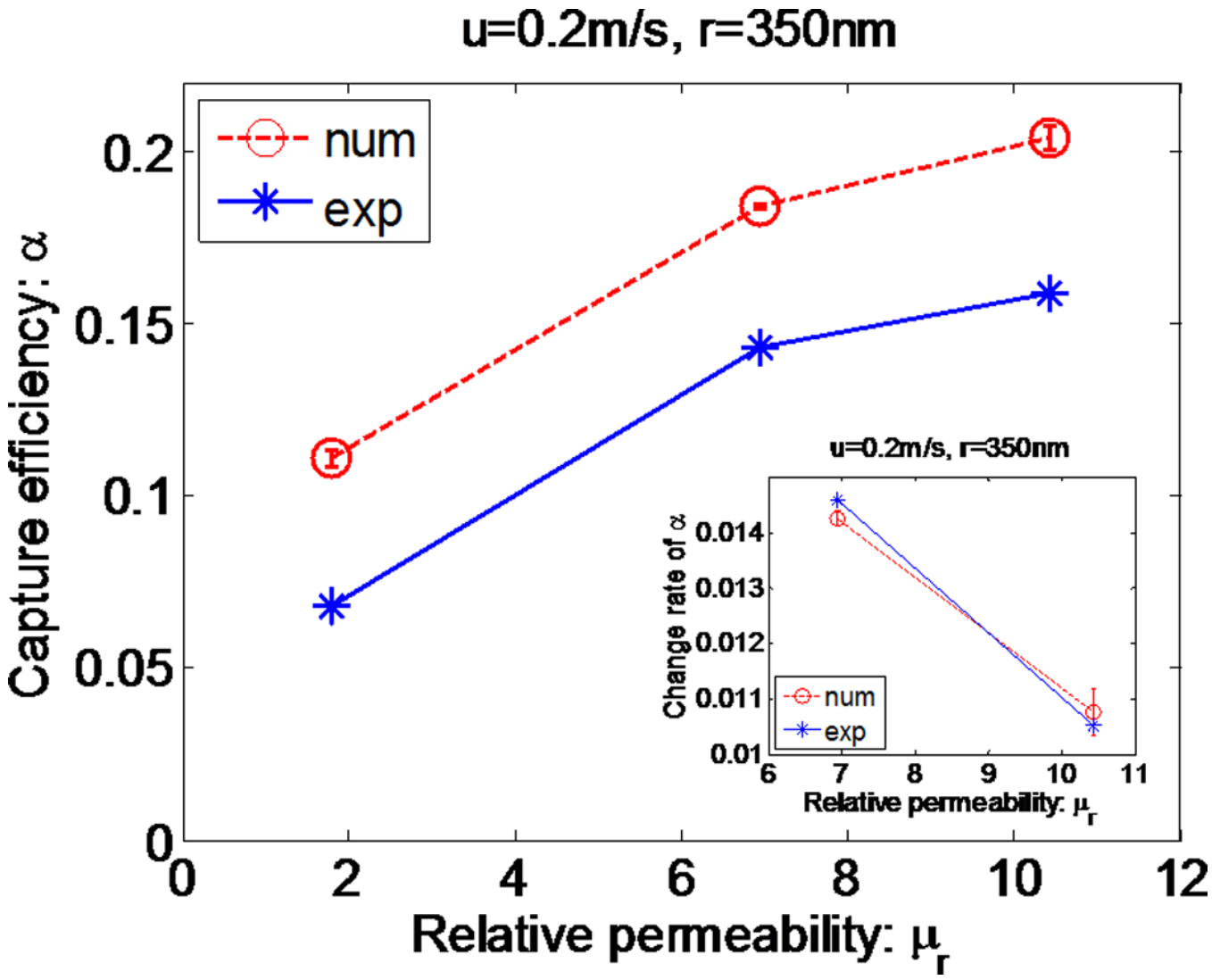

Fig. 2.

Capture efficiency for stents of various relative permeability, with u=0.2 m/s and r=350 nm. The inset shows the normalized capture efficiency, which is defined as ratio of capture efficiency to that in the reference case of μ_r=1.8. Solid line represents experimental results in Forbe's work and dashed line represents numerical results. Error bars stand for standard error.

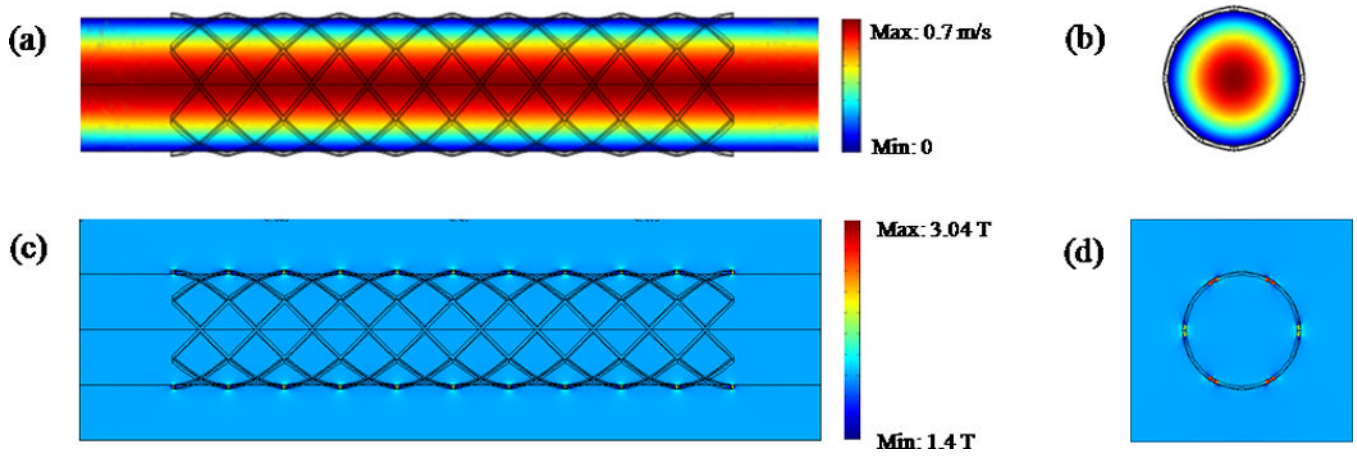

Fig. 3.

(a) Flow velocity distribution across the channel. The flow velocity ranges from 0 m/s to 0.7 m/s as indicated by the color bar; (b) Cross section view of flow velocity; (c) Magnetic flux density distribution across the system. The magnetic flux density ranges from 1.4 T to 3.04 T as shown in the color bar; (d) Cross section view of magnetic field

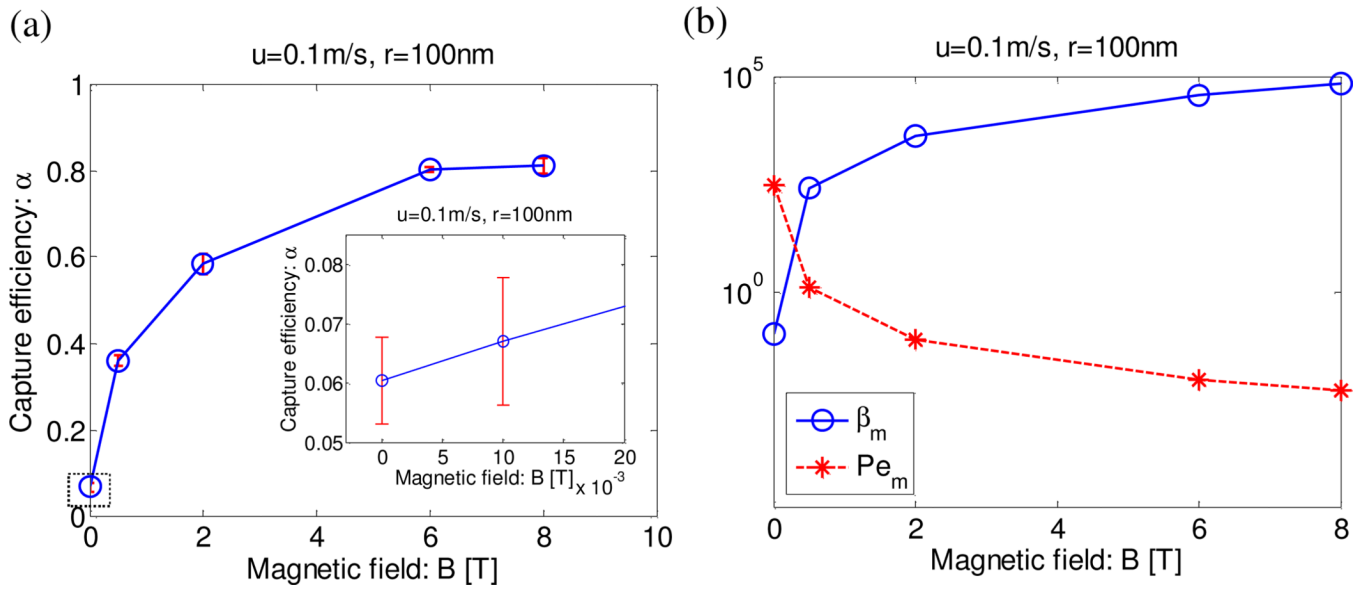

Fig. 4.

(a) Capture efficiency under various magnetic fields, with u=0.1 m/s and r=100 nm. The inset magnifies the results under the magnetic field of 0 T and 0.01 T; (b) β_m and Pe_m in terms of magnetic fields under the same situation as (a)

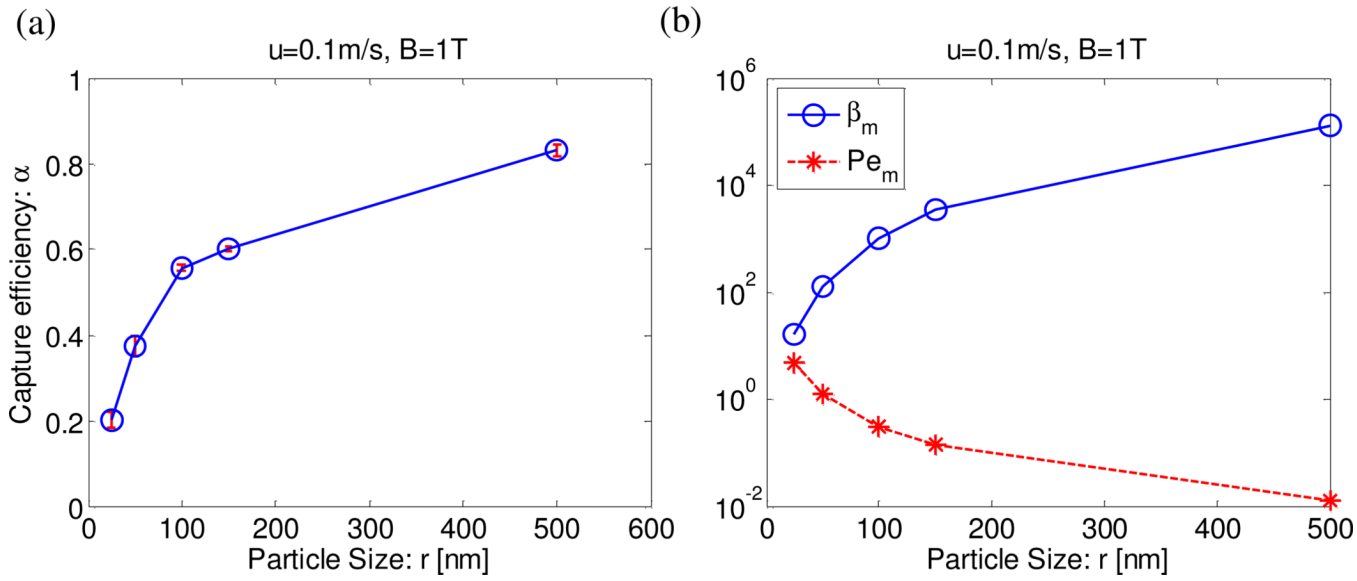

Fig. 5.

(a) Capture efficiency of particle of various sizes, with u=0.1 m/s and B=1 T; (b) β_m and Pe_m in terms of particle sizes under the same situation as (a)

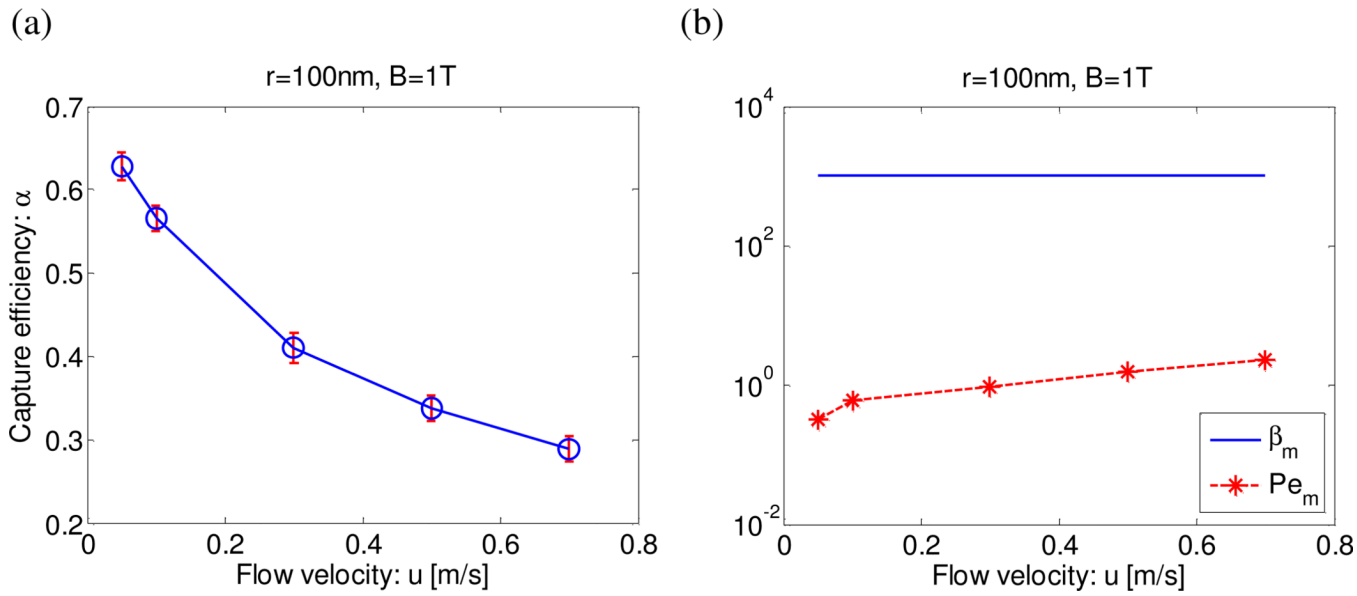

Fig. 6.

(a) Capture efficiency under various flow velocities, with r=100 nm and B=1 T; (b) β_m and Pe_m in terms of flow velocities under the same situation as (a)

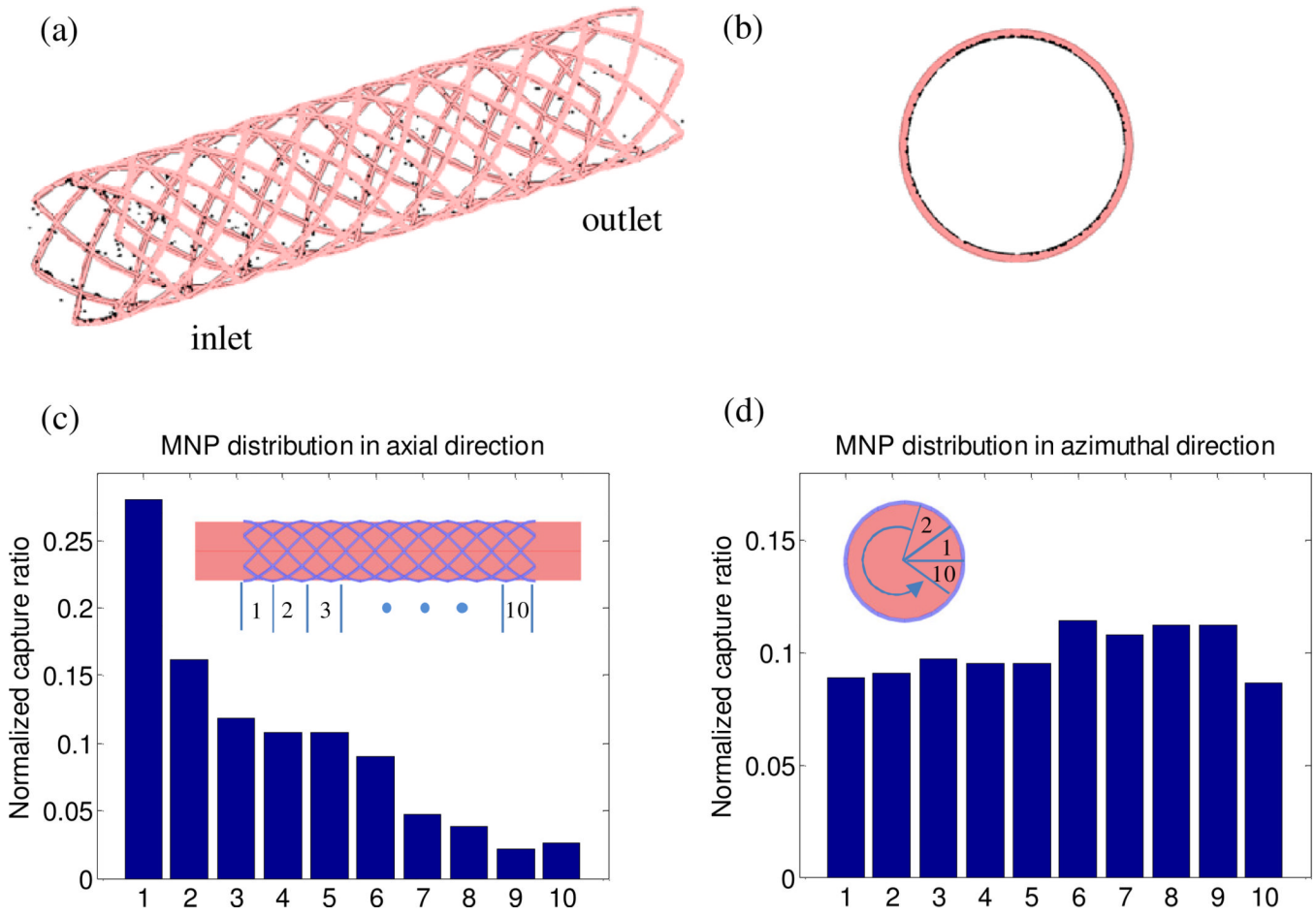

Fig. 7.

(a) Distribution of captured MNPs (dots in the figure) in the vessel (only MNPs and stents are shown). The capture ratio decreases from inlet (left) to outlet (right). (b) Cross section view of the distribution of captured MNPs. (c) Normalized capture ratio of MNPs along the axial direction. The inset shows the stented region is divided into 10 equal regions in the axial direction, numbering from 1 to 10. (d) Normalized capture ratio of MNPs along azimuthal direction. The inset shows the cross-section region is also divided into 10 equal sections along azimuthal direction.

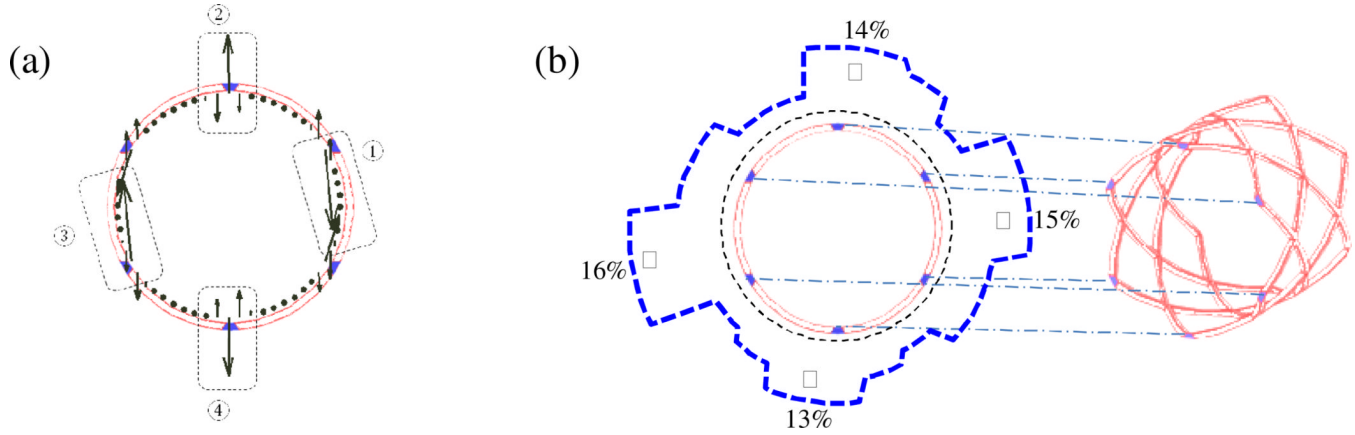

Fig. 8.

(a) Magnetic force distribution in the beginning section of the stented region. Arrows show the magnitude and direction of the magnetic force near the inner channel surface. (b) Ratio distribution of captured MNPs in the azimuthal direction. The blue bold dashed line illustrates the normalized value of capture ratio of MNPs in the section of stented regions. The circular dashed line marks zero ratio of captured MNPs. The stent struts are corresponded in two views using dot-dash lines. In order to make the figure more concise, the stent is plotted partially.